JEM Journal of Experimental Medicine

BRIEF DEFINITIVE REPORT

Endothelial cell fitness dictates the source of regenerating liver vasculature

Mahak Singhal[1,2,3]*, Xiaoting Liu[4,5]*, Donato Inverso[1], Kai Jiang[4], Jianing Dai[4], Hao He[4,5], Susanne Bartels[1], Weiping Li[5,6], Ashik Ahmed Abdul Pari[1,2,3], Nicolas Gengenbacher[1,3], Eva Besemfelder[1], Lijian Hui[6], Hellmut G. Augustin[1,2,7]**, and Junhao Hu[4]**

Neoangiogenesis plays a key role in diverse pathophysiological conditions, including liver regeneration. Yet, the source of new endothelial cells (ECs) remains elusive. By analyzing the regeneration of the liver vasculature in irradiation-based myeloablative and nonmyeloablative bone marrow transplantation mouse models, we discovered that neoangiogenesis in livers with intact endothelium was solely mediated by proliferation of resident ECs. However, following irradiation-induced EC damage, bone marrow–derived mononuclear cells were recruited and incorporated into the vasculature. Further experiments with direct bone marrow infusion or granulocyte colony–stimulating factor (G-CSF)–mediated progenitor cell mobilization, which resembles clinically relevant stem cell therapy, demonstrated that bone marrow–derived cells did not contribute to the regeneration of liver vasculature after two-thirds partial hepatectomy (PHx). Taken together, the data reconcile many of the discrepancies in the literature and highlight that the cellular source of regenerating endothelium depends on the fitness of the residual vasculature.

Introduction

Successive processes of vasculogenesis and angiogenesis form the embryonic vasculature. In adults, the blood vessels remain largely quiescent. Nevertheless, they play a central role in maintaining tissue homeostasis (Hu et al., 2014; Rafii et al., 2016; Augustin and Koh, 2017). During tissue repair and pathophysiological conditions like tumor growth or cardiovascular diseases, the formation of new blood vessels was long believed to result from the expansion of resident endothelial cells (ECs) of neighboring vessels (Chung and Ferrara, 2011). Yet, a growing number of studies suggest that a small population of bone marrow–derived mononuclear cells (BMDMCs), which express a variety of endothelial surface markers and have thus been designated as endothelial progenitor cells, could promote neovascularization in adults (Asahara et al., 1997; Shi et al., 1998; Peichev et al., 2000; Wang et al., 2012). Based on these compelling preclinical findings, it was hypothesized that diseases involving a deficient adult neovascularization should benefit from a bone marrow–based cellular therapy.

The adult liver is the only organ that can completely regenerate after injury or partial resection. This remarkable feature has led to the development of innovative therapeutic strategies: partial hepatectomy (PHx) for patients with early-stage resectable hepatocellular carcinoma, and split or living donor liver transplantation for patients with end-stage liver disease (Clavien et al., 2007; Michalopoulos, 2007, 2017). The successful evaluation of bone marrow–based cellular therapies in preclinical liver regenerative models (Almeida-Porada et al., 2010; DeLeve, 2013) promoted clinical trials with either autologous bone marrow transplants or mobilization of stem/progenitor cells with the administration of G-CSF (Forbes et al., 2015). Results from initial uncontrolled clinical trials indicated increased serum albumin levels and an overall improvement in several clinical parameters such as the Child-Pugh-Turcotte score or the model for end-stage liver disease score (Huebert and Rakela, 2014). However, in a recent randomized, controlled phase 2 trial involving 81 patients with compensated liver cirrhosis, administration of G-CSF alone or in combination with hematopoietic stem cell (HSC) infusion failed to improve liver function or to ameliorate fibrosis (Newsome et al., 2018). These contradictory clinical observations highlight a lack of understanding of the mechanism of action of

[1]Division of Vascular Oncology and Metastasis Research, German Cancer Research Center Heidelberg (DKFZ-ZMBH Alliance), Heidelberg, Germany; [2]European Center for Angioscience, Medical Faculty Mannheim, Heidelberg University, Heidelberg, Germany; [3]Faculty of Biosciences, Heidelberg University, Heidelberg, Germany; [4]Interdisciplinary Research Center on Biology and Chemistry, Shanghai Institute of Organic Chemistry, Chinese Academy of Sciences, Shanghai, China; [5]University of Chinese Academy of Sciences, Beijing, China; [6]State Key Laboratory of Cell Biology, CAS Center for Excellence in Molecular Cell Science, Institute of Biochemistry and Cell Biology, Shanghai Institutes for Biological Sciences, Chinese Academy of Sciences, Shanghai, China; [7]German Cancer Consortium, Heidelberg, Germany.

*M. Singhal and X. Liu contributed equally to this work; **H.G. Augustin and J. Hu contributed equally to this work; Correspondence to Hellmut G. Augustin: augustin@angiogenese.de; Junhao Hu: jhhu@sioc.ac.cn.

different cell therapies as well as their relative cellular contribution to the regenerating tissue (Forbes and Newsome, 2016). To date, it remains controversial if BMDMCs can physically incorporate into the regenerative vasculature or if they merely stimulate liver regeneration via secretion of paracrine-acting factors (Bautch, 2011; Medina et al., 2017; Dickson, 2018). Hence, it is necessary to use better preclinical liver regeneration models that allow quantitative assessment of BMDMC contribution to the newly formed blood vessels in clinically relevant pathophysiological settings.

We have in the present study employed multiple irradiation-based myeloablative and nonmyeloablative mouse models that allowed us to unambiguously evaluate the contribution of different cellular sources to the regenerating liver vasculature following two-thirds PHx. These definite experiments revealed that BMDMCs do not incorporate into the liver vasculature under nonvascular-damaging conditions. Based on these findings, we hypothesized that in patients with intact liver endothelium, bone marrow–based cellular therapies will not contribute to liver vascular regeneration. Indeed, bone marrow transplant, as well as G-CSF–mediated stem cell mobilization experiments, revealed that regeneration of liver vasculature relies primarily on preexisting intact liver ECs.

Results and discussion

BMDMCs incorporate in the irradiation-damaged liver vasculature

In adult mice, the liver is able to restore its original mass and structure within 10 d following PHx. Thereby, it uniquely enabled us to trace ECs in newly formed blood vessels of the regenerating liver. We initially employed bone marrow chimeras in which GFP$^+$ Lin$^-$Sca-1$^+$Kit$^+$ (LSK) bone marrow cells, which consist of HSCs and multipotent progenitor cells that are able to fully reconstitute the bone marrow, were transplanted into lethally irradiated syngeneic WT recipients (Fig. S1 A). 1 mo later, bone marrow chimeric mice (Fig. S1 B) were subjected to PHx to induce liver regeneration, and the liver vasculature was analyzed 10 d after PHx. In line with a previous study (Wang et al., 2012), a fraction of GFP$^+$ cells was found incorporated into the liver vasculature (Fig. S1 C, upper panel). Surprisingly, though, GFP$^+$ ECs were also detectable in livers of sham-operated mice (Fig. S1 C, lower panel; Fig. 1 A; and Video 1), suggesting that bone marrow–recruited cells had incorporated into the liver vasculature independent of the PHx-induced regenerative burst, possibly as a result of irradiation-induced vascular damage. The number of GFP$^+$ ECs in PHx mice was ∼1.8× higher as compared with the sham-operated mice (Fig. S1 D). However, this observation could be attributed either to an increased recruitment of GFP$^+$ BMDMCs or to a higher proliferation of bone marrow–derived cells following PHx. A microarray analysis comparing the bone marrow–recruited ECs and the corresponding resident liver ECs revealed that BMDMCs incorporated as bona fide liver ECs after irradiation (Fig. S1 E). However, the bone marrow–derived ECs retained expression of a few stem cell lineage genes (Fig. S1 E), indicating their cell of origin. Further, the bone marrow–derived ECs showed similar expression of cell cycle regulatory genes when compared with the resident liver ECs (Fig. S1, F and G), indicating that both cell populations possess a similar proliferation capacity. These data demonstrate that bone marrow–derived ECs are functionally indistinguishable from the resident liver ECs.

The majority of previous studies investigated the contribution of BMDMCs in irradiation-conditioned bone marrow chimeric mice (Asahara et al., 1997; Mathews et al., 2004; Zhang et al., 2014). However, the effect of irradiation on the liver vasculature has not been taken into consideration. To investigate why irradiation-based conditioning induced BMDMC incorporation into the liver vasculature, WT mice were irradiated with 9 Gy. As early as 2 h after irradiation, a strong phosphorylation of histone H2A.X (Ser139), a marker of double-strand DNA breaks, was detected in the nuclei of both hepatocytes and ECs (Fig. 1, B and C). We hypothesized that the observed DNA damage might cause EC apoptosis. Concurrently, liver ECs were found positive for the apoptotic marker cleaved caspase-3 following irradiation (Fig. 1, D and E), which is in line with a previous study (Langley et al., 1997), suggesting that ECs are sensitive to irradiation exposure. Quantitative PCR analysis revealed higher expression of *Bax*, an apoptotic activator, in livers of irradiated but not partially hepatectomized mice compared with nonirradiated and partially hepatectomized mice (Fig. 1 F). Interestingly, *Icam1* was highly upregulated in livers of irradiated mice as compared with the PHx group (Fig. 1 G). It was previously demonstrated that apoptotic ECs upregulate *Icam1* expression, resulting in enhanced BMDMC recruitment and vascular incorporation (Gao et al., 2008; Bhatwadekar et al., 2009). Thus, our results demonstrate that irradiation induced EC double-strand DNA breaks and apoptosis, which eventually led to impaired endothelial self-repair. Consequently, transplantation of healthy bone marrow into a preirradiated host resulted in BMDMC recruitment and incorporation as bona fide liver ECs to restore the injured endothelium.

To generate bone marrow chimeras without damaging the liver vasculature, a radio-protective shield was applied over the upper abdomen while irradiating the animals (Halder et al., 1998; Fig. 2 A). To quantitatively evaluate whether BMDMCs incorporate into the liver vasculature following irradiation, GFP$^+$ bone marrow cells were transplanted into lethally irradiated recipients. Mice receiving 9 Gy whole-body irradiation in the presence of a liver shield had a strong reduction of GFP$^+$ BMDMCs in their livers as compared with mice irradiated without a liver shield (Fig. 2 B). This observation was confirmed by flow cytometry–based analysis revealing a reduction of the GFP$^+$ liver EC fraction from 3.85% in mice without a liver shield to 0.4% in mice with a liver shield (Fig. 2 C). Thus, the observed induction of phosphorylated histone H2A.X and cleaved caspase-3 after irradiation, as well as the significantly reduced incorporation of GFP$^+$ BMDMCs into the liver vasculature by a liver shield, clearly shows that whole-body irradiation had caused catastrophic damage to the liver vasculature, which led to an emergency recruitment and incorporation of bone marrow–derived cells for tissue repair and rejuvenation of organ function. These data hint at a reparative role of bone marrow cells following irradiation damage, which was similarly reported for irradiation-caused injury of the central nervous system (Dietrich et al., 2018) and the bone marrow stromal niche (Abbuehl et al., 2017).

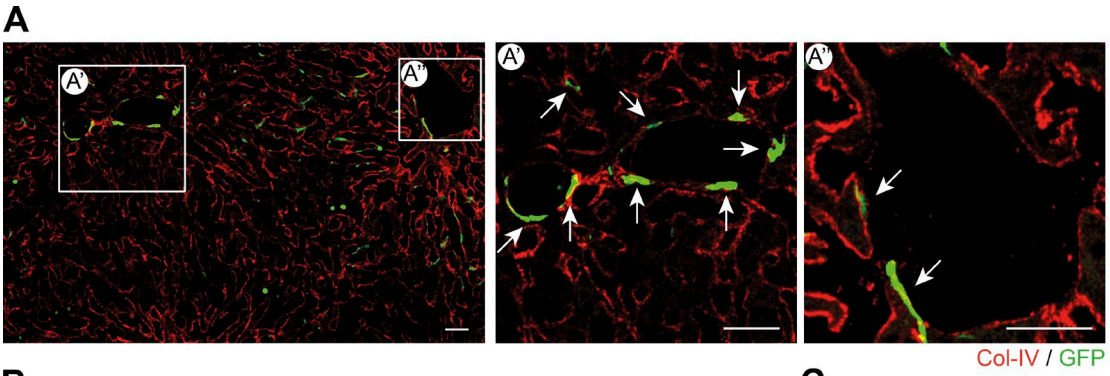

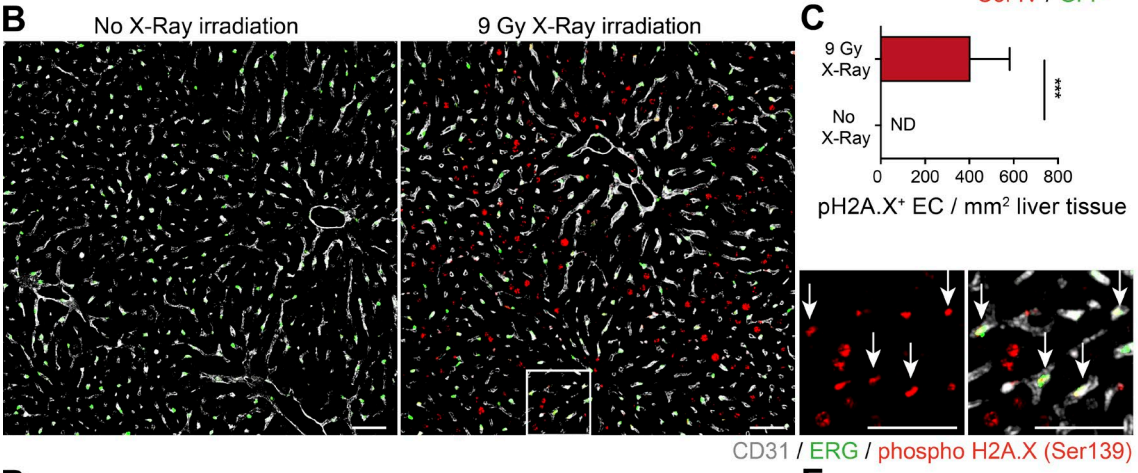

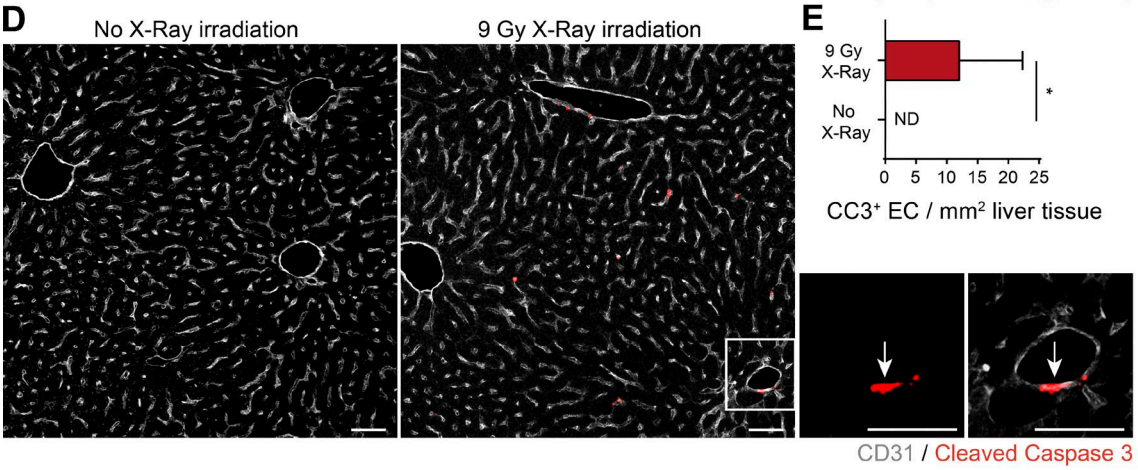

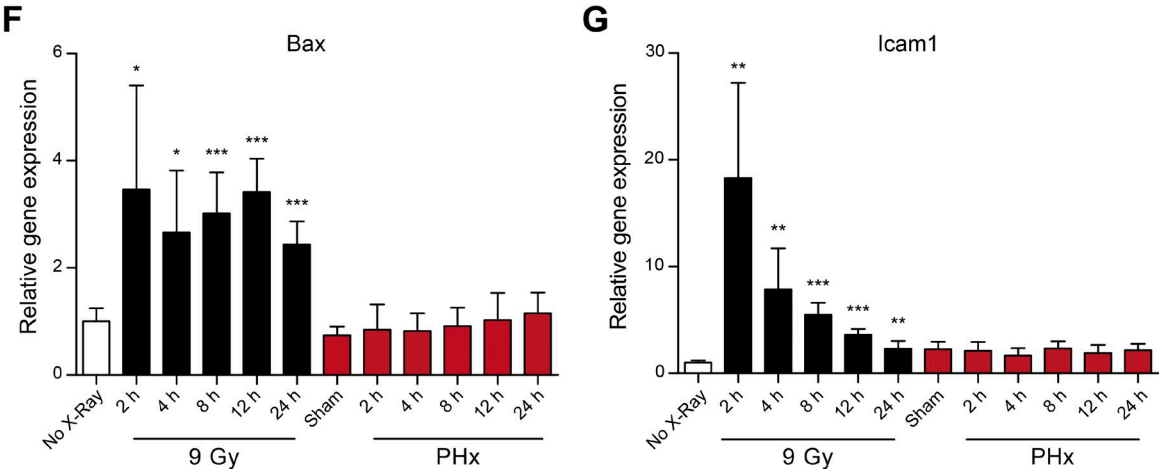

BMDMCs do not incorporate in the intact vasculature during liver regeneration

To circumvent the limitations of irradiation, the contribution of GFP⁺ BMDMCs to vascular expansion following PHx was further analyzed in three nonmyeloablative models: (1) parabiotic pairs of WT and GFP-expressing mice, (2) bone marrow chimera in *Rag2*$^{-/-}\gamma_c^{-/-}$*Kit*$^{W/Wv}$ animals, and (3) *VECad-Cre*^{ERT2}*xRosa26-YFP*$^{fl/fl}$ mice. First, a parabiotic experiment was performed with syngeneic WT and CAG-GFP mice (Fig. 3 A; Kamran et al., 2013). In both WT (Para-WT) and CAG-GFP (Para-GFP) mice, approximately half of the mononuclear fraction of blood, which contains endothelial progenitor cells (Aoki et al., 2004), was GFP⁺, indicating that the circulatory systems of the two mice had successfully fused (Fig. S2 A). We hypothesized that if BMDMCs contribute to the regenerating vasculature, then there should be GFP⁺ ECs incorporated into the regenerated liver in Para-WT mice after PHx. To induce maximal liver regeneration in the parabiotic mice, both Para-WT and Para-GFP mice were simultaneously subjected to PHx. Flow cytometry analysis revealed no increase of GFP⁺ ECs in the livers of hepatectomized Para-WT (Para-WT-PHx) mice compared with the livers of sham-operated Para-WT (Para-WT-Sham) mice (Fig. 3 B). Most of the GFP⁺ cells in the livers of Para-WT-PHx mice were CD45⁺ and maintained their hematopoietic identity (Fig. S2, B and C). Similarly, there was no significant decrease in the GFP⁺ fraction of liver ECs in Para-GFP-PHx mice as compared with Para-GFP-Sham mice (Fig. 3 B). Further, staining for the proliferation marker Ki67 demonstrated that the proliferating ECs in Para-WT mice were GFP⁻ resident ECs (Fig. 3 C and Fig. S2 D).

To further examine the contribution of BMDMCs during liver regeneration, YFP⁺ LSK cells were transplanted into *Rag2*$^{-/-}\gamma_c^{-/-}$*Kit*$^{W/Wv}$ mice. These mice lack T and B cells (*Rag2*$^{-/-}$) and natural killer cells ($\gamma_c^{-/-}$, common gamma chain of the *Il2r*) and have an impaired HSC self-renewal capacity (*Kit*$^{W/Wv}$). They are thereby able to accept HSCs without prior irradiation (Waskow et al., 2009; Fig. 3 D). Bone marrow chimeric mice (Fig. 3 E) were subjected to PHx to induce liver regeneration. The regenerated livers of *Rag2*$^{-/-}\gamma_c^{-/-}$*Kit*$^{W/Wv}$ mice showed a similar vascular microstructure as WT controls 10 d after PHx, suggesting that liver regeneration was not impaired in *Rag2*$^{-/-}\gamma_c^{-/-}$*Kit*$^{W/Wv}$ mice (Fig. S2 E). The YFP⁺ EC ratio of both the resected and the regenerated liver lobes of an individual mouse was analyzed to precisely evaluate the contribution of YFP⁺ BMDMCs to vascular regeneration. However, the percentage of YFP⁺ ECs among total liver ECs was found to be unaltered before and 10 d after PHx (Fig. 3 F), indicating that YFP⁺ BMDMCs did not integrate into the regenerating liver vasculature following PHx. Thus, these data demonstrate that bone marrow–derived cells did not physically incorporate into the regenerating liver vasculature after PHx under nonvascular-damaging conditions.

After ruling out the direct contribution of BMDMCs in two independent nonirradiation-conditioned preclinical models, we investigated the contribution of terminally differentiated resident ECs to the regeneration of liver vasculature upon PHx. To this end, we applied a fate mapping strategy with *VECad-Cre*^{ERT2}*xRosa26-YFP*$^{fl/fl}$ mice, in which transient tamoxifen administration resulted in permanent YFP labeling of the adult vasculature (Fig. 3 G). Consistent with a previous report (Höfer et al., 2016), the *VECad* promoter was specifically active in ECs and silenced in the hematopoietic compartment of adult mice. The tamoxifen administration in adult *VECad-Cre*^{ERT2}*xRosa26-YFP*$^{fl/fl}$ mice successfully labeled the liver vasculature with YFP (Fig. S2 F). However, neither LSK cells in the bone marrow nor mononuclear cells in the peripheral blood were YFP labeled (Fig. S2, G and H). Following a resting period of 4 wk after tamoxifen administration, these mice were subjected to PHx to induce liver regeneration. There were no significant changes in the frequencies of YFP⁺ liver ECs while performing an indexed analysis comparing resected and regenerated liver lobes of six individual mice (Fig. 3 H). Additional labeling of proliferating cells with EdU revealed YFP⁺ resident ECs to be proliferation efficient, as they constituted up to 95% of the EdU⁺ liver EC population (Fig. 3 I). In concordance with the other two nonmyeloablative models, the data demonstrate that liver vasculature depended on differentiated resident ECs during PHx-induced liver regeneration. Likewise, resident ECs were previously reported to mediate adult neovascularization following cardiac injury (He et al., 2017) and during tumor progression (Peters et al., 2005; Purhonen et al., 2008). Interestingly, a subset of liver ECs coexpressing CD157 and CD200 was recently identified as tissue-resident vascular endothelial stem cells that are capable of local clonal expansion and thereby can support neovascularization during liver repair (Wakabayashi et al., 2018). Similar findings have recently been reported during large vessel regeneration in an aortic injury model (McDonald et al., 2018). Thus, under nonvascular-damaging conditions, the vascular regeneration proceeds exclusively by the expansion of preexisting tissue-resident ECs.

Liver neovascularization during chronic liver damage

To substantiate our findings from acute PHx-induced liver regeneration in chronic liver damage models, liver neovascularization was further analyzed in *VECad-Cre*^{ERT2}*xRosa26-YFP*$^{fl/fl}$ mice after either repeated administration of carbon tetrachloride (CCl_4) or a single injection of empty adenovirus. First, *VECad-Cre*^{ERT2}*xRosa26-YFP*$^{fl/fl}$ mice with labeled ECs were in-

Figure 1. **Irradiation-based myeloablation induces EC injury and primes for BMDMC incorporation. (A)** Representative images of liver sections of irradiation-conditioned GFP⁺ bone marrow–transplanted sham-operated mice. **(A' and A'')** Zoomed-in images illustrating GFP⁺ cells incorporated into the liver vasculature. Arrows indicate GFP⁺ ECs. Scale bars, 100 µm. For complete confocal reconstruction, see Video 1. **(B)** Representative images of liver sections of control or irradiated mice costained with phospho-H2A.X (Ser139), CD31 (EC-specific surface marker), and ERG (EC-specific nuclear marker). Zoomed-in images are shown on the right. Arrows indicate phospho-H2A.X (Ser139)–positive ECs. Scale bars, 50 µm. **(C)** The plot shows the count of pH2A.X⁺ ECs per 1 mm^2 of liver tissue (mean ± SD, n = 6 mice). **(D)** Representative images of liver sections of control or irradiated mice costained with cleaved caspase-3 (CC3) and CD31 (EC-specific surface marker). Zoomed-in images are shown on the right. Arrows indicate CC3⁺ ECs. Scale bars, 50 µm. **(E)** The plot shows the count of CC3⁺ ECs per 1 mm^2 of liver tissue (mean ± SD, n = 6 mice). **(F and G)** Quantitative PCR analysis of mRNA expression of *Bax* (F) and *Icam1* (G) in livers of mice after irradiation or PHx (mean ± SD, n = 5–6 mice for each time point). ND, nondetectable; *, P < 0.05; **, P < 0.01; ***, P < 0.001 (two-tailed Student's t test).

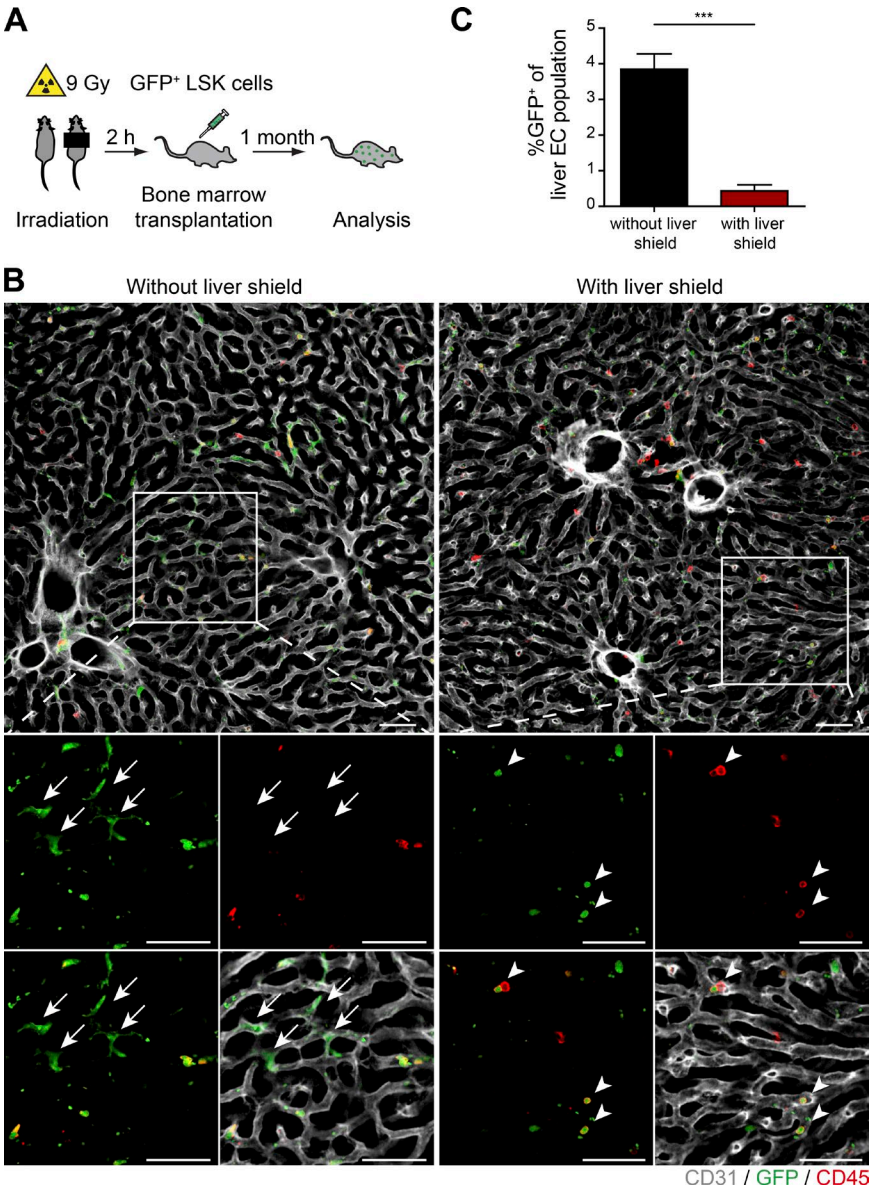

Figure 2. **A radioprotective shield reduces the recruitment of BMDMCs to the liver vasculature.** **(A)** Experimental outline of PHx-induced liver regeneration in irradiation-conditioned GFP+ bone marrow–transplanted mice in the absence or presence of a liver shield. **(B)** Mice were irradiated with or without liver shield. Representative images of liver sections of bone marrow chimeric mice costained with GFP, CD45, and CD31 (EC-specific surface marker). Zoomed-in images are shown at the bottom. Arrows indicate GFP+ ECs. Arrowheads indicate GFP+ hematopoietic cells in the shielded liver. Scale bars, 50 µm. **(C)** The percentage of GFP+ ECs in livers of mice irradiated in the presence or absence of a liver shield was analyzed by FACS (mean ± SD, n = 6 mice). ***, $P < 0.001$ (two-tailed Student's t test).

jected with either oil or CCl_4 to induce liver injury over a period of 4 wk. A strong increase in plasma alanine aminotransferase/aspartate aminotransferase (ALT/AST) levels was observed after CCl_4 treatment, indicating liver damage (Fig. S3 A). Following a recovery period of 2 wk after CCl_4 treatment, Sirius red staining was performed on the liver sections of CCl_4-treated mice, which showed a strong deposition of collagen, an indication of liver fibrosis (Fig. S3 B). Further, flow cytometry analysis revealed no significant changes in the frequencies of YFP+ liver ECs between mice treated with either oil or CCl_4 (Fig. S3 C). Next, *VECad-Cre^{ERT2}xRosa26-YFP$^{fl/fl}$* mice with labeled ECs were injected with 10^{11} viral particles of empty replication-deficient adenovirus. This causes an early cytopathic effect on hepatocytes and a secondary adaptive immune response against infected hepatocytes during later stages of the experiment, as illustrated by enhanced plasma ALT/AST values (Fig. S3 D). 6 wk after adenovirus infection, flow cytometry analysis showed no significant alterations in YFP positivity of liver ECs when comparing adenovirus-infected to PBS-injected control mice (Fig. S3 E). Thus, the data from both chronic liver damage models coherently demonstrate that intact endothelium is self-sufficient for tissue repair.

Bone marrow–based cellular therapies fail to promote liver vascular regeneration

Bone marrow–derived cells have previously been reported to supposedly constitute ∼25% of total liver ECs following PHx (Wang et al., 2012; DeLeve, 2013). These compelling preclinical observations have stimulated clinical stem cell therapeutic approaches for patients with end-stage liver disease. Initial case studies and proof-of-concept trials with the administration of autologous stem cell grafts showed improvement in liver function and accelerated hepatic regeneration (Huebert and Rakela, 2014; Moore et al., 2014). However, a subsequent randomized controlled trial involving 58 patients with decompensated alcoholic liver disease resulted in no additional benefit from autologous BMDMC infusion combined with standard medical therapy

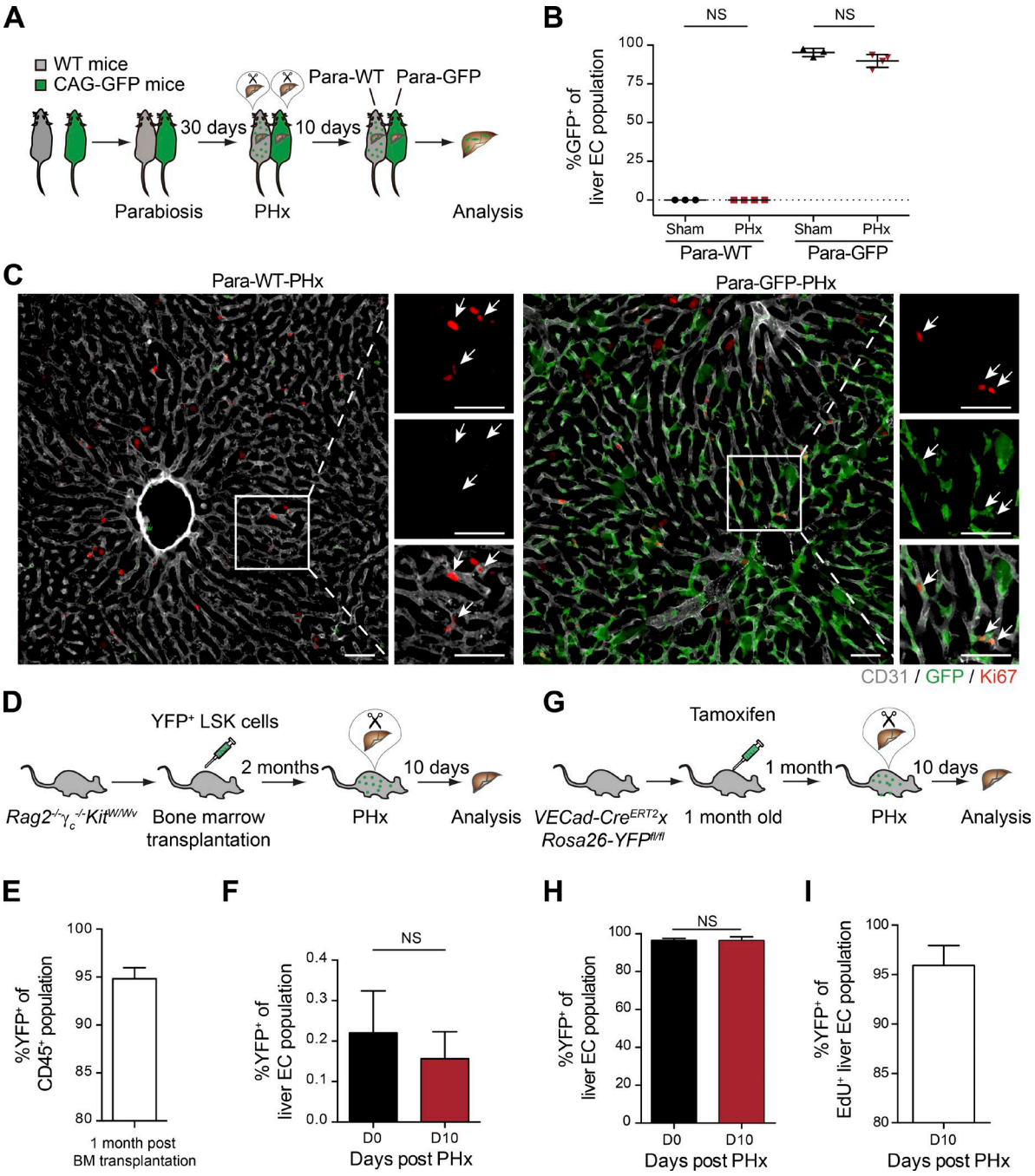

Figure 3. **BMDMCs do not contribute to the regeneration of liver vasculature in nonmyeloablative models. (A)** Experimental outline of the parabiotic model. The circulatory systems of WT and CAG-GFP mice were surgically conjoined, and both mice were subjected to PHx to induce liver regeneration. **(B)** The ratio of GFP+ ECs in the livers of Para-WT (sham operated and PHx) as well as Para-GFP (sham operated and PHx) mice was analyzed by FACS (mean ± SD, *n* = 3–4 mice). **(C)** Representative images of liver sections of Para-WT-PHx or Para-GFP-PHx mice costained with Ki67, GFP, and CD31 (EC-specific surface marker). Zoomed-in images are shown on the right. Arrows indicate Ki67+ ECs. Scale bars, 50 µm. **(D)** Experimental outline for transplantation of LSK cells into *Rag2*$^{-/-}$*γc*$^{-/-}$*Kit*$^{W/Wv}$ mice. **(E)** FACS analysis of donor chimerism in CD45+ cells from peripheral blood of *Rag2*$^{-/-}$*γc*$^{-/-}$*Kit*$^{W/Wv}$ recipients (mean ± SD, *n* = 4 mice). **(F)** The percentage of YFP+ ECs in the livers of *Rag2*$^{-/-}$*γc*$^{-/-}$*Kit*$^{W/Wv}$ mice before and 10 d after PHx was analyzed by FACS (mean ± SD, *n* = 4 mice). **(G)** Experimental outline of the *VECad-Cre*^{ERT2}*xRosa26-YFP*$^{fl/fl}$ genetic labeling model. **(H)** The frequency of YFP+ ECs in livers of the same *VECad-Cre*^{ERT2}*xRosa26-YFP*$^{fl/fl}$ mouse before and 10 d after PHx was analyzed by FACS (mean ± SD, *n* = 6 mice). **(I)** The proportion of YFP+ cells among the total proliferated liver ECs (as labeled by EdU) after PHx (mean ± SD, *n* = 6 mice). Two-tailed Student's *t* test.

as compared with standard medical therapy alone (Spahr et al., 2013). Likewise, the phase 2 REALISTIC trial with 81 randomly assigned liver cirrhosis patients concluded that the addition of G-CSF and stem cell infusion did not improve liver dysfunction as compared with standard care alone (Newsome et al., 2018). To quantitatively assess the physical contribution of bone marrow–based cellular therapies to liver vascular regeneration, we employed direct infusion of bone marrow cells or administration of

G-CSF to mobilize BMDMCs after PHx, which closely resembles clinical conditions. To this end, YFP-labeled bone marrow cells, consisting of ∼20,000 LSK cells, were injected via tail vein into the NOD-scid gamma (NSG) mice on day 2 after PHx (Fig. 4 A), i.e., before proliferation of liver ECs. In line with a previous report (Verbiest et al., 2016), the NSG mice successfully accepted the allograft, as there were ∼15% YFP$^+$ cells among total circulating CD45$^+$ cells in the peripheral blood on day 10 following PHx (Fig. 4 B). Circulating YFP$^+$ cells could infiltrate into the liver tissue, as they constituted around 25% of the CD45$^+$ population in the livers of BM-transplanted NSG mice (Fig. 4 B). Yet, when comparing the livers of PHx and sham-operated animals, there was no significant incorporation of YFP$^+$ cells among total liver ECs (Fig. 4 C). Further, immunofluorescence analysis revealed that there were YFP$^+$ cells in the liver tissue; however, they exclusively maintained their hematopoietic identity (Fig. 4, D and E). High-resolution image analysis failed to identify a significant number of YFP$^+$ liver ECs in the regenerated liver, clearly suggesting that the infused bone marrow cells do not directly contribute to the regeneration of the liver vasculature.

To expand and mobilize endogenous BMDMCs, Neulasta (PEGylated G-CSF), a clinically approved agent for mobilizing hematopoietic progenitor cells (Hopman and DiPersio, 2014), was injected in WT mice on day 2 following PHx (Fig. 5 A). There was a strong increase in the number of circulating LSK cells in G-CSF–injected mice as compared with saline-injected control mice (Fig. 5 B). Circulating liver EC progenitors were reported to express CD133 (Harb et al., 2009), and the infusion of CD133$^+$ BMDMCs could accelerate liver regeneration (Wang et al., 2012). Yet, we did not observe any significant expansion or recruitment of CD133$^+$ liver ECs when comparing PHx to sham-operated mice following G-CSF administration (Fig. 5 C). High-resolution three-dimensional image analysis revealed that CD133 staining in the liver tissue was exclusively restricted to epithelial cells of bile ducts (Fig. 5 D). Further, we did not detect a CD133$^+$ fraction of the liver EC, which was previously described as sinusoidal progenitor cells (Wang et al., 2012), in either sham-operated or PHx mice. These data recapitulate the observations from the REALISTIC trial, as neither direct infusion of bone marrow cells in NSG mice nor G-CSF–mediated mobilization of progenitor cells in WT mice showed any BMDMC contribution to the regenerating liver vasculature. Our data clearly suggest that stem cell infusion/mobilization therapies do not physically contribute to the regeneration of liver vasculature in mice with healthy remaining vasculature. Yet, BMDMCs might contribute through other mechanisms toward liver regeneration, e.g., by differentiating into other cellular compartments in the liver or by improving liver function via paracrine signals. Additionally, our data cannot exclude the impact of the immune system on the success of BMDMC contribution toward liver parenchyma. Future studies involving stringent and mechanistic preclinical experimental approaches will need to address these questions to possibly establish a scientific rationale for bone marrow cell–involved stem cell therapies to interfere with liver dysfunction.

In summary, using a wide array of lineage-tracing tools, the present study was aimed at unveiling the source of newly formed vessels during liver regeneration. Our data demonstrate that (1) irradiation causes irreversible damage to the liver vasculature, thereby restricting the proliferative capacity of residing liver ECs and resulting in recruitment and incorporation of BMDMCs for vascular repair; (2) under nonvascular-damaging conditions, reconstitution of the liver vasculature relies on preexisting vessels with no direct contribution of BMDMCs; and (3) systemically infused bone marrow cells or G-CSF–mobilized progenitor cells do not integrate into the regenerating liver vasculature after PHx. In conclusion, by unraveling under which conditions BMDMCs may contribute to vascular regeneration, the present study reconciles many of the discrepancies in the published literature regarding the cellular source of liver neovascularization. We conclude that both preexisting liver ECs and BMDMCs can act as a potential source of new vessels depending on the vascular fitness.

Materials and methods

Mouse experiments

C57BL/6N (WT) and NSG mice were purchased from Charles River. CAG-GFP (chicken β-actin promoter and cytomegalovirus enhancer regulate expression of enhanced GFP) mice were purchased from the Jackson Laboratory. *Rag2*$^{-/-}\gamma_c^{-/-}$*Kit*$^{W/Wv}$ mice were generated as described previously (Waskow et al., 2009). C57BL/6 *Rosa26-YFP*$^{fl/fl}$ mice were crossed with C57BL/6 *VECad-Cre*^{ERT2} mice to specifically label ECs upon tamoxifen application. Male mice (8–10 wk of age) were used in this study unless otherwise indicated. All mice were housed on a 12-h light/dark cycle with free access to food and drinking water in specific pathogen–free animal facilities. All animal experiments were approved by the institutional and governmental Animal Care and Use Committees (IRCBC-2016-02 to J. Hu and G220/11, G213/17, and G219/17 to H.G. Augustin from Regierungspräsidium Karlsruhe, Germany). All experiments were performed in accordance with the institutional guidance for the care and use of laboratory animals.

PHx

PHx was performed according to the methods described by Mitchell and Willenbring (2008) to induce liver regeneration. In brief, mice were anaesthetized with a mixture of ketamine (100 mg/kg body weight) and xylazine (10 mg/kg body weight). Then, the left lateral lobe and the median lobe were ligated with 4–0 silk sutures and resected. The mice were kept for 10 d to regenerate the lost liver mass. Finally, the mice were euthanized, and livers were collected for FACS analysis or immunostaining.

Transplantation of HSCs without irradiation

PanRosa^{YFP} mice were used as donors. Bone marrow cells of *PanRosa*^{YFP} mice were flushed from femurs, tibias, coxae, and humeri using PBS supplemented with 5% heat-inactivated FCS. Cells were filtered through a 40-µm cell strainer (Falcon). Fc receptors were blocked by incubating cells in 5% FCS with purified mouse IgG (500 mg/ml; Jackson ImmunoResearch). All stainings were performed in 5% FCS on ice for 30 min with optimal dilutions of commercially prepared antibodies. Reagents used were CD3ε PE (145-C11), CD11b PE (M1/70), CD45R PE (RA3-6B2), CD117 eFluor780 (2B8), Sca-1 PerCP-Cy5.5 (D7; eBiosciences), CD4 PE (H129.19), CD8a PE (53–6.7), CD19 PE (1D3), Gr-1 PE (RB6-8C5), NK1.1 PE (PK136), and Ter119 PE (Ter119; BD Pharmingen). The

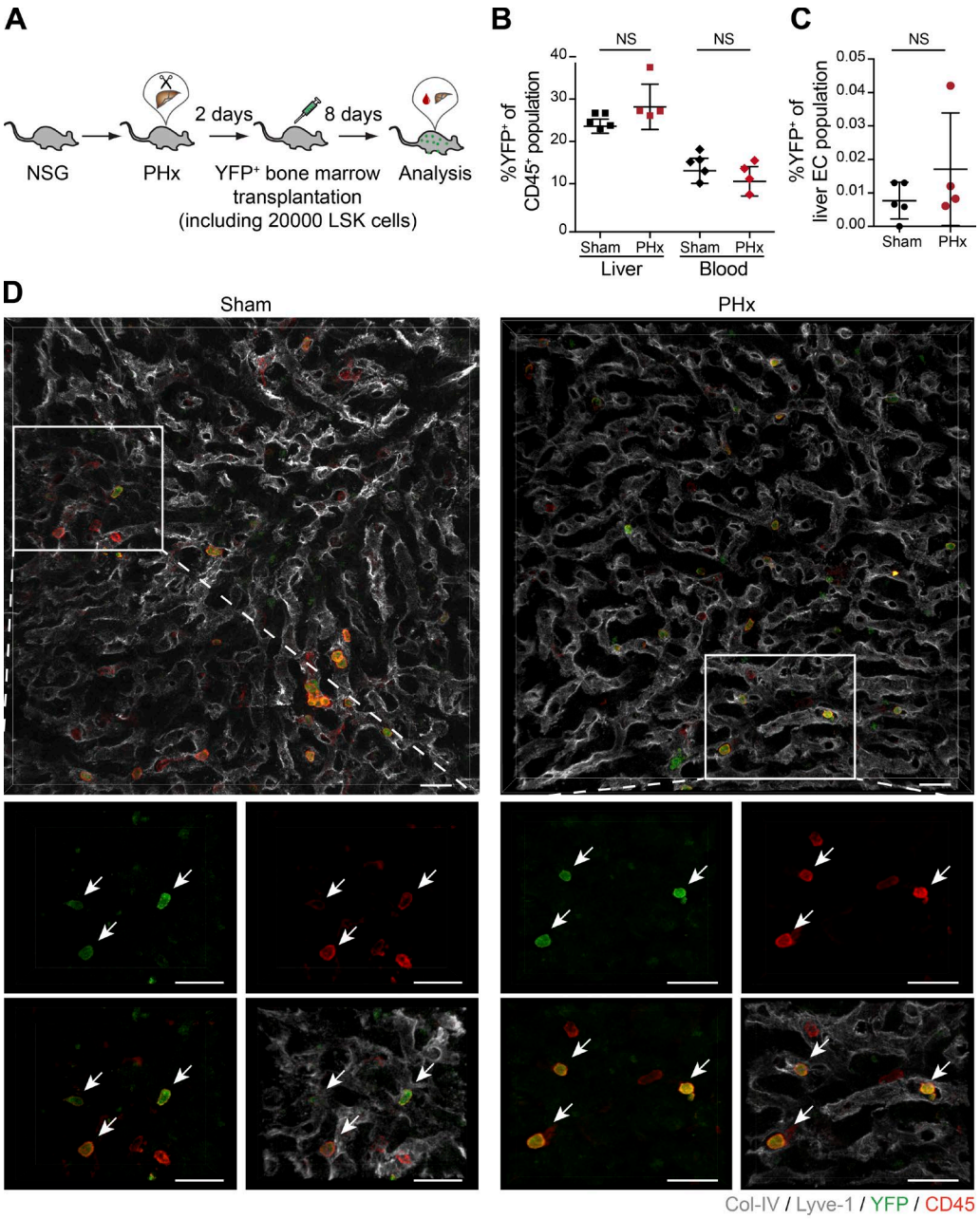

E

	YFP+ (n ± SD)	YFP+ CD45+ (n ± SD)	YFP+ EC (n ± SD)
Sham	249 ± 66.57	248 ± 65.91	0.8 ± 0.84
PHx	245 ± 64	244 ± 64	0.25 ± 1

Figure 4. **Infused bone marrow cells do not incorporate into the regenerating liver vasculature. (A)** Experimental outline of PHx-induced liver regeneration in NSG mice. Prior to the angiogenic phase (on day 2 after PHx), mice were infused intravenously with YFP-labeled bone marrow cells as a regenerative cellular therapy. **(B)** The frequency of YFP+ hematopoietic cells (CD45+) in the liver and the peripheral blood of sham-operated and PHx mice was analyzed by FACS (mean ± SD, *n* = 4–5 mice). **(C)** The ratio of YFP+ ECs in the livers of sham-operated and PHx mice was analyzed by FACS (mean ± SD, *n* = 4–5 mice). **(D)** Representative images of liver sections of sham-operated and PHx mice costained with YFP, CD45, and liver EC–specific marker (Lyve-1/Col-IV). Zoomed-in images are shown at the bottom. Arrows indicate YFP+ cells. All traced YFP+ cells were positive for CD45 but negative for EC markers. Scale bars, 25 µm. **(E)** Shown are the absolute numbers of YFP+ cells, YFP+ hematopoietic cells, and YFP+ ECs counted per 1 mm^2 of the liver tissue of sham-operated and PHx mice (mean ± SD, *n* = 4–5 mice). Two-tailed Student's *t* test.

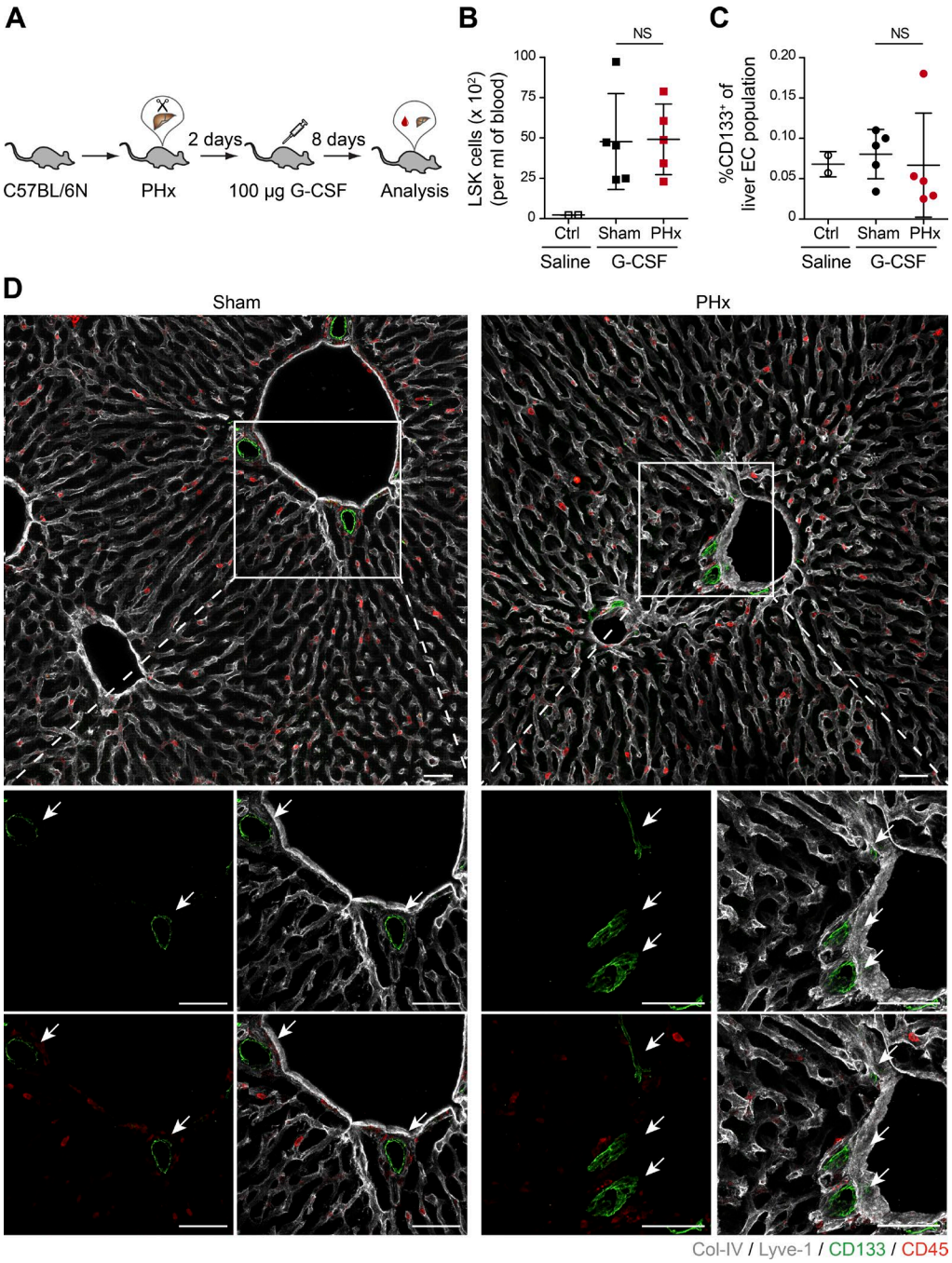

Figure 5. **G-CSF–mobilized bone marrow cells do not incorporate into the regenerating liver vasculature. (A)** Experimental outline of PHx-induced liver regeneration in C57BL/6N mice. Prior to the angiogenic phase (on day 2 after PHx), mice were injected subcutaneously with 100 µg G-CSF (as a regenerative therapy) to mobilize bone marrow–derived progenitor cells. **(B)** The frequency of circulating LSK cells in the peripheral blood of sham-operated and PHx mice was analyzed by FACS (mean ± SD, $n = 5$ mice). **(C)** The ratio of CD133⁺ ECs in the livers of sham-operated and PHx mice was analyzed by FACS (mean ± SD, $n = 5$ mice). **(B and C)** Saline-injected mice served as controls. **(D)** Representative images of liver sections of sham-operated and PHx mice costained with CD133 (progenitor cell marker), CD45, and liver EC–specific marker (Lyve-1/Col-IV). Zoomed-in images are shown at the bottom. Arrows indicate CD133⁺ cells. All traced CD133⁺ cells were negative for CD45 and EC markers. Scale bars, 50 µm. Two-tailed Student's *t* test.

lineage cocktail was composed of CD3ε, CD4, CD8a, CD11b, CD19, CD45R, Gr-1, NK1.1, and Ter119. Dead cells were excluded by staining with Sytox Blue (Invitrogen). Approximately 5,000 LSK cells were sorted by FACSAriaIII (Becton Dickinson) and injected intravenously into nonirradiated triple transgenic *Rag2*$^{-/-}\gamma_c^{-/-}$*Kit*$^{W/Wv}$ recipient mice. Donor chimerism of blood cells was determined 1 mo after transplantation.

Irradiation and bone marrow transplantation

8-wk-old WT mice were lethally irradiated with a total dose of 9 Gy (split dose, 2 × 4.5 Gy). For liver shield experiments, 8-wk-old WT mice were first anaesthetized by a ketamine/xylazine mixture. Then, a customized circular lead plate was put over the upper abdomen of the mouse to protect the liver from irradiation. After a 2-h rest, the mice were injected with bone marrow cells or 5,000

LSK cells isolated from CAG-GFP transgenic mice via the tail vein. 1 mo later, mice were subjected to two-thirds PHx. The resected liver lobes were isolated and subjected to FACS analysis and cryopreservation, respectively. 10 d after PHx, the regenerated livers were resected and analyzed. Donor chimerism in the bone marrow of recipient animals was determined after sacrificing animals.

Microarray analysis

For gene expression analysis, microarrays were performed by the German Cancer Research Center Genomics Core Facility. Briefly, liver ECs were isolated from irradiation-conditioned bone marrow chimeric mice for surface marker expression ($DAPI^-$ $CD45^-$ $CD31^+$ $CD146^+$). Further, liver ECs were segregated based on YFP expression (YFP^-: resident liver ECs; YFP^+: bone marrow–derived liver ECs). Thereafter, RNA was isolated with the Arcturus PicoPure RNA Isolation Kit (Life Technologies), and RNA quality and quantity were analyzed on an Agilent Bioanalyzer. Next, cDNA was hybridized on mouse Clariom S assay (Applied Biosystems) according to the manufacturer's protocol. Microarray data were normalized and analyzed with the Chipster software. The microarray data with the description are deposited under GEO accession no. GSE116377.

Parabiosis

To fuse the blood circulation of two independent mice, female WT and CAG-GFP mice were subjected to parabiotic surgery as described previously (Kamran et al., 2013). In brief, mice were anaesthetized with 1.5% isoflurane. A longitudinal skin incision was made to expose the elbow and knee joint. Then, the elbows and knee joints of the two mice were bound together with surgical sutures. Afterwards, the skins of the two mice were sewn together. To prevent infection and to relieve pain, the skin wounds were treated with hydrogel containing lincomycin hydrochloride (5 mg/g) and lidocaine (4 mg/g) for 3 d. 1 mo later, blood was collected from the tail veins of all the operated mouse pairs for FACS analysis to confirm the blood chimerism. To induce liver regeneration, both mice of the operated pairs were subjected to two-thirds PHx. 10 d later, the mice were euthanized, and the regenerated livers of WT mice and CAG-GFP mice were analyzed.

Constitutive labeling of ECs in *VECad-Cre^{ERT2}xRosa26-YFP$^{fl/fl}$* mice

4–5-wk-old animals were administered four doses of tamoxifen (100 mg/kg) twice a week. The animals were rested for 1 mo after tamoxifen application. Afterwards, mice were subjected to two-thirds PHx. The resected and regenerated liver lobes of an individual mouse were analyzed with flow cytometry. To label the proliferating liver ECs after PHx, EdU (40 mg/kg) was administered intraperitoneally daily during the angiogenic phase of liver regeneration (days 2–6). The regenerated liver lobes were stained with an EdU Flow Cytometry Kit (Baseclick GmbH) and analyzed by FACS.

Chronic liver injury models

The CCl_4 model

VECad-Cre^{ERT2}xRosa26-YFP$^{fl/fl}$ mice with labeled ECs were intraperitoneally injected with either peanut oil alone or in combination with CCl_4 (0.7 µl/g body weight) three times a week for a duration of 4 wk (Scholten et al., 2015). After the last treatment, mice were allowed to recover for 2 wk, and, thereafter, mice were euthanized, and livers were collected for FACS analysis or immunostaining. Mice were bled, and plasma ALT/AST levels were monitored during the course of the experiment.

Adenovirus-mediated liver damage

VECad-Cre^{ERT2}xRosa26-YFP$^{fl/fl}$ mice with labeled ECs were intravenously injected with either PBS or 10^{11} viral particles of empty replication-deficient adenovirus (VB180308-1016nff; VectorBuilder Inc.). Afterward, mice were bled at regular intervals, and plasma ALT/AST levels were monitored. Once the ALT/AST levels subsided, mice were euthanized, and livers were collected for FACS analysis or immunostaining.

Regenerative therapy

Direct infusion of YFP-labeled stem cells

Whole bone marrow cells were isolated from *PanRosa^{YFP}* mice as described above. On day 2 after PHx or sham operation, the NSG mice were injected intravenously with suspension of bone marrow cells (consisting of 20,000 LSK cells). After 8 d, the mice were euthanized, and blood and livers were collected for FACS analysis or immunostaining.

G-CSF–mediated bone marrow–derived progenitor mobilization

On day 2 after PHx or sham operation, the mice were injected with 100 µg of Neulasta (PEG-G-CSF) subcutaneously. After 8 d, the mice were euthanized, and bone marrow, blood, and livers were collected for FACS analysis or immunostaining.

Flow cytometry analysis

Blood chimerism

Blood samples were drawn from the tail veins and kept in anticoagulant EDTA-K_2–coated tubes. Erythrocytes were lysed with 1× ACK (ammonium chloride potassium) lysis buffer, and the remaining cells were collected by centrifugation at 500 *g* for 5 min. Cells were resuspended with PBS and analyzed by flow cytometry. Cells were gated based on size and granularity. Then the percentage of YFP^+/GFP^+ cells within the mononuclear population was determined.

Liver EC incorporation

Livers were collected and minced into small pieces and incubated with collagenase I buffer (200 U/ml collagenase I, 0.01% $CaCl_2$, and 1.25% DNase in DMEM) for 30 min at 37°C with agitation. The cell suspension was filtered through a 100-µm cell strainer before being centrifuged twice at 50 *g* for 2 min to remove the hepatocytes. The cell suspension was further treated with 5 ml 1× ACK lysis buffer to remove erythrocytes. After centrifugation, the cells were incubated in staining solution with antibodies CD45-PE (#561087; BD Pharmingen), CD45-APC-Cy7 (#557659; BD Pharmingen), CD31-APC (#551262; BD Pharmingen), CD133-FITC (#11-1331-82; eBioscience), and CD146-PerCP-Vio700 (#130-103-865; Miltenyi Biotec). All stainings were performed in 5% FCS (in PBS) on ice for 30 min with optimal dilutions of commercially prepared antibodies. For FACS analysis, $DAPI^+$ dead cells were first excluded, and $CD45^-CD31^+CD146^+$ populations were defined as liver ECs. Finally, the percentage of GFP^+ or YFP^+ cells in the liver EC population was measured using either Beckman Coulter Cytoflex or BD Canto-II.

Immunostaining and image analysis

Livers were fixed in 4% PFA overnight. 50-µm sections were prepared with a vibratome (Leica VT1000S). Sections were blocked and permeabilized with PBS containing 10% normal donkey serum and 0.3% Triton for 2 h at room temperature. Sections were then incubated with primary antibodies overnight at 4°C, followed by fluorophore-conjugated secondary antibodies for 2 h at room temperature. Images were taken with a Leica SP8 confocal microscope. The following antibodies were used in this study: rabbit anti-mouse Lyve-1 (#103-PA50AG; Reliatech), hamster anti-mouse CD31 (MA3105; Thermo Scientific), rabbit anti-mouse cleaved caspase-3 (9661; Cell Signaling Technology), rabbit anti-mouse phospho-histone H2A.X (9718; Cell Signaling Technology), rabbit anti-mouse Ki-67 (12202; Cell Signaling Technology), rabbit anti-mouse collagen-IV (polyclonal; Abcam), rat anti-mouse CD133-FITC (#11-1331-82; eBioscience), rat anti-mouse CD45 (#CL9446APl; Cedarlane Laboratories), donkey anti-rabbit IgG-Rhodamine Red-X (711–296-152; Jackson ImmunoResearch), donkey anti-rabbit IgG–Alexa Fluor 647 (711–606-152; Jackson ImmunoResearch), goat anti-Armenian hamster IgG-Rhodamine Red-X (127–295-160; Jackson ImmunoResearch), and goat anti-Armenian hamster IgG–Alexa Fluor 488 (127–545-160; Jackson ImmunoResearch). All stainings were performed with optimal dilutions recommended by the manufacturer.

For Video 1, a semiautomatic surface rendering module in Imaris (Bitplane) was used to create three-dimensional volumetric surface objects corresponding either to individual cells or to the liver vascular system.

Comparative gene expression

Total RNA was extracted from the livers of irradiated or hepatectomized mice using a Trizol isolation system (Thermo Scientific) according to the manufacturer's instructions. RNA was transcribed into cDNA using the ReverTra Ace qPCR RT Master Mix with gDNA Remover (Toyobo). Quantitative PCR was performed with SYBR Green Master Mix (Invitrogen). Primers (*Bax*: 5′-AGACAGGGGCCTTTTTGCTAC-3′, forward, and 5′-AATTCGCCGGAGACACTCG-3′, reverse; *Icam1*: 5′-CTGGATCTC AGGCCGCAAG-3′, forward, and 5′-TGTCGAGCTTTGGGATGG TAG-3′, reverse) were ordered from Sangon Biotech. Gene expression levels were calculated based on the Delta-Delta Ct relative quantification method. mRNA levels were normalized to β-actin expression.

Statistical analyses

P values were determined by two-tailed Student's *t* test. Values of $P < 0.05$ were considered statistically significant. Error bars represent mean ± SD.

Online supplemental material

Fig. S1 shows that BMDMCs incorporate into the liver vasculature in irradiation-conditioned bone marrow chimeric mice. It includes microarray-based gene expression analyses to compare the resident and the bone marrow–derived liver ECs. Fig. S2 contains validation data for different nonmyeloablative models employed to lineage trace liver ECs after PHx. Fig. S3 includes data from chemical- and immune-mediated chronic liver injury models. Video 1 illustrates three-dimensional reconstruction of the liver vasculature of the sham-operated mouse 1 mo after irradiation-conditioned bone marrow transplantation.

Acknowledgments

The authors would like to thank Prof. Dr. Hans-Reimer Rodewald (German Cancer Research Center, Heidelberg, Germany) for providing *Rag2*$^{-/-}\gamma_c^{-/-}$*Kit*$^{W/Wv}$ mice. We thank Prof. Dr. Franklin Constantini (Columbia University, New York, NY) for providing *Rosa26-YFP*$^{fl/fl}$ mice. We thank Dr. Katrin Busch and Dr. Kay Klapproth (German Cancer Research Center) for the fruitful discussions and their critical comments on the manuscript. We are most grateful for the excellent technical support of the Flow Cytometry, Genomics, Light Microscopy, and Laboratory Animal Facilities of the German Cancer Research Center and Interdisciplinary Research Center of Biology and Chemistry.

This work was supported by grants from the Deutsche Forschungsgemeinschaft for projects SFB-873, "Maintenance and differentiation of stem cells in development and disease" (TP B6 to H.G. Augustin), and SFB-TR209, "Hepatocellular carcinoma" (TP C3 to H.G. Augustin); the European Union FP7 project "Early warning signals of aging in human stem cells and age-related disorders" (306240 to H.G. Augustin); the European Research Council Advanced Grant "AngioMature" (787181 to H.G. Augustin); Research Training Group 2099 "Hallmarks of Skin Cancer" (TP P8 to H.G. Augustin); and the National Science Foundation of China (31571203 to J. Hu). J. Hu is supported by the Thousand Young Talents Recruitment Program. D. Inverso is supported by the European Molecular Biology Organization long-term fellowship program (EMBO ALTF 1018-2016).

The authors declare no competing financial interests.

Author contributions: M. Singhal, X. Liu, H.G. Augustin, and J. Hu conceived and designed the study. M. Singhal and X. Liu performed most of the experiments. S. Bartels contributed to the irradiation-primed bone marrow transplantation model. K. Jiang and H. He contributed to the parabiosis experiments, cell isolation, and FACS analysis. W. Li and L. Hui contributed to the mouse model of irradiation-induced liver injury. D. Inverso and M. Singhal performed Imaris-based image analysis. J. Dai, N. Gengenbacher, A.A. Abdul Pari, and E. Besemfelder provided technical help. M. Singhal, X. Liu, H.G. Augustin, and J. Hu analyzed and interpreted data. H.G. Augustin and J. Hu supervised the project. M. Singhal, H.G. Augustin, and J. Hu wrote the manuscript. All authors discussed the results and commented on the manuscript.

Submitted: 2 January 2018
Revised: 6 July 2018
Accepted: 17 August 2018

References

Abbuehl, J.P., Z. Tatarova, W. Held, and J. Huelsken. 2017. Long-term engraftment of primary bone marrow stromal cells repairs niche damage and improves hematopoietic stem cell transplantation. *Cell Stem Cell.* 21:241–255.e6. https://doi.org/10.1016/j.stem.2017.07.004

Almeida-Porada, G., E.D. Zanjani, and C.D. Porada. 2010. Bone marrow stem cells and liver regeneration. *Exp. Hematol.* 38:574–580. https://doi.org/10.1016/j.exphem.2010.04.007

Aoki, M., M. Yasutake, and T. Murohara. 2004. Derivation of functional endothelial progenitor cells from human umbilical cord blood mononuclear cells isolated by a novel cell filtration device. *Stem Cells.* 22:994–1002. https://doi.org/10.1634/stemcells.22-6-994

Asahara, T., T. Murohara, A. Sullivan, M. Silver, R. van der Zee, T. Li, B. Witzenbichler, G. Schatteman, and J.M. Isner. 1997. Isolation of putative progenitor endothelial cells for angiogenesis. *Science.* 275:964–967. https://doi.org/10.1126/science.275.5302.964

Augustin, H.G., and G.Y. Koh. 2017. Organotypic vasculature: From descriptive heterogeneity to functional pathophysiology. *Science.* 357:eaal2379. https://doi.org/10.1126/science.aal2379

Bautch, V.L. 2011. Stem cells and the vasculature. *Nat. Med.* 17:1437–1443. https://doi.org/10.1038/nm.2539

Bhatwadekar, A.D., J.V. Glenn, T.M. Curtis, M.B. Grant, A.W. Stitt, and T.A. Gardiner. 2009. Retinal endothelial cell apoptosis stimulates recruitment of endothelial progenitor cells. *Invest. Ophthalmol. Vis. Sci.* 50:4967–4973. https://doi.org/10.1167/iovs.09-3616

Chung, A.S., and N. Ferrara. 2011. Developmental and pathological angiogenesis. *Annu. Rev. Cell Dev. Biol.* 27:563–584. https://doi.org/10.1146/annurev-cellbio-092910-154002

Clavien, P.A., H. Petrowsky, M.L. DeOliveira, and R. Graf. 2007. Strategies for safer liver surgery and partial liver transplantation. *N. Engl. J. Med.* 356:1545–1559. https://doi.org/10.1056/NEJMra065156

DeLeve, L.D. 2013. Liver sinusoidal endothelial cells and liver regeneration. *J. Clin. Invest.* 123:1861–1866. https://doi.org/10.1172/JCI66025

Dickson, I. 2018. Stem cells: Stem cell therapy for liver cirrhosis unREALIS TIC? *Nat. Rev. Gastroenterol. Hepatol.* 15:4.

Dietrich, J., N. Baryawno, N. Nayyar, Y.K. Valtis, B. Yang, I. Ly, A. Besnard, N. Severe, K.U. Gustafsson, O.C. Andronesi, et al. 2018. Bone marrow drives central nervous system regeneration after radiation injury. *J. Clin. Invest.* 128:281–293. https://doi.org/10.1172/JCI90647

Forbes, S.J., and P.N. Newsome. 2016. Liver regeneration - mechanisms and models to clinical application. *Nat. Rev. Gastroenterol. Hepatol.* 13:473–485. https://doi.org/10.1038/nrgastro.2016.97

Forbes, S.J., S. Gupta, and A. Dhawan. 2015. Cell therapy for liver disease: From liver transplantation to cell factory. *J. Hepatol.* 62(1, Suppl):S157–S169. https://doi.org/10.1016/j.jhep.2015.02.040

Gao, D., D.J. Nolan, A.S. Mellick, K. Bambino, K. McDonnell, and V. Mittal. 2008. Endothelial progenitor cells control the angiogenic switch in mouse lung metastasis. *Science.* 319:195–198. https://doi.org/10.1126/science.1150224

Halder, R.C., S. Seki, A. Weerasinghe, T. Kawamura, H. Watanabe, and T. Abo. 1998. Characterization of NK cells and extrathymic T cells generated in the liver of irradiated mice with a liver shield. *Clin. Exp. Immunol.* 114:434–447. https://doi.org/10.1046/j.1365-2249.1998.00726.x

Harb, R., G. Xie, C. Lutzko, Y. Guo, X. Wang, C.K. Hill, G.C. Kanel, and L.D. DeLeve. 2009. Bone marrow progenitor cells repair rat hepatic sinusoidal endothelial cells after liver injury. *Gastroenterology.* 137:704–712. https://doi.org/10.1053/j.gastro.2009.05.009

He, L., X. Huang, O. Kanisicak, Y. Li, Y. Wang, Y. Li, W. Pu, Q. Liu, H. Zhang, X. Tian, et al. 2017. Preexisting endothelial cells mediate cardiac neovascularization after injury. *J. Clin. Invest.* 127:2968–2981. https://doi.org/10.1172/JCI93868

Höfer, T., K. Busch, K. Klapproth, and H.R. Rodewald. 2016. Fate mapping and quantitation of hematopoiesis in vivo. *Annu. Rev. Immunol.* 34:449–478. https://doi.org/10.1146/annurev-immunol-032414-112019

Hopman, R.K., and J.F. DiPersio. 2014. Advances in stem cell mobilization. *Blood Rev.* 28:31–40. https://doi.org/10.1016/j.blre.2014.01.001

Hu, J., K. Srivastava, M. Wieland, A. Runge, C. Mogler, E. Besemfelder, D. Terhardt, M.J. Vogel, L. Cao, C. Korn, et al. 2014. Endothelial cell-derived angiopoietin-2 controls liver regeneration as a spatiotemporal rheostat. *Science.* 343:416–419. https://doi.org/10.1126/science.1244880

Huebert, R.C., and J. Rakela. 2014. Cellular therapy for liver disease. *Mayo Clin. Proc.* 89:414–424. https://doi.org/10.1016/j.mayocp.2013.10.023

Kamran, P., K.I. Sereti, P. Zhao, S.R. Ali, I.L. Weissman, and R. Ardehali. 2013. Parabiosis in mice: a detailed protocol. *J. Vis. Exp.* (80). https://doi.org/10.3791/50556

Langley, R.E., E.A. Bump, S.G. Quartuccio, D. Medeiros, and S.J. Braunhut. 1997. Radiation-induced apoptosis in microvascular endothelial cells. *Br. J. Cancer.* 75:666–672. https://doi.org/10.1038/bjc.1997.119

Mathews, V., P.T. Hanson, E. Ford, J. Fujita, K.S. Polonsky, and T.A. Graubert. 2004. Recruitment of bone marrow-derived endothelial cells to sites of pancreatic beta-cell injury. *Diabetes.* 53:91–98. https://doi.org/10.2337/diabetes.53.1.91

McDonald, A.I., A.S. Shirali, R. Aragón, F. Ma, G. Hernandez, D.A. Vaughn, J.J. Mack, T.Y. Lim, H. Sunshine, P. Zhao, et al. 2018. Endothelial regeneration of large vessels is a biphasic process driven by local cells with distinct proliferative capacities. *Cell Stem Cell.* 23:210–225.e6. https://doi.org/10.1016/j.stem.2018.07.011

Medina, R.J., C.L. Barber, F. Sabatier, F. Dignat-George, J.M. Melero-Martin, K. Khosrotehrani, O. Ohneda, A.M. Randi, J.K.Y. Chan, T. Yamaguchi, et al. 2017. Endothelial progenitors: A consensus statement on nomenclature. *Stem Cells Transl. Med.* 6:1316–1320. https://doi.org/10.1002/sctm.16-0360

Michalopoulos, G.K. 2007. Liver regeneration. *J. Cell. Physiol.* 213:286–300. https://doi.org/10.1002/jcp.21172

Michalopoulos, G.K. 2017. Hepatostat: Liver regeneration and normal liver tissue maintenance. *Hepatology.* 65:1384–1392. https://doi.org/10.1002/hep.28988

Mitchell, C., and H. Willenbring. 2008. A reproducible and well-tolerated method for 2/3 partial hepatectomy in mice. *Nat. Protoc.* 3:1167–1170. https://doi.org/10.1038/nprot.2008.80

Moore, J.K., B.M. Stutchfield, and S.J. Forbes. 2014. Systematic review: the effects of autologous stem cell therapy for patients with liver disease. *Aliment. Pharmacol. Ther.* 39:673–685. https://doi.org/10.1111/apt.12645

Newsome, P.N., R. Fox, A.L. King, D. Barton, N.N. Than, J. Moore, C. Corbett, S. Townsend, J. Thomas, K. Guo, et al. 2018. Granulocyte colony-stimulating factor and autologous CD133-positive stem-cell therapy in liver cirrhosis (REALISTIC): an open-label, randomised, controlled phase 2 trial. *Lancet Gastroenterol. Hepatol.* 3:25–36. https://doi.org/10.1016/S2468-1253(17)30326-6

Peichev, M., A.J. Naiyer, D. Pereira, Z. Zhu, W.J. Lane, M. Williams, M.C. Oz, D.J. Hicklin, L. Witte, M.A. Moore, and S. Rafii. 2000. Expression of VEGFR-2 and AC133 by circulating human CD34(+) cells identifies a population of functional endothelial precursors. *Blood.* 95:952–958.

Peters, B.A., L.A. Diaz, K. Polyak, L. Meszler, K. Romans, E.C. Guinan, J.H. Antin, D. Myerson, S.R. Hamilton, B. Vogelstein, et al. 2005. Contribution of bone marrow-derived endothelial cells to human tumor vasculature. *Nat. Med.* 11:261–262. https://doi.org/10.1038/nm1200

Purhonen, S., J. Palm, D. Rossi, N. Kaskenpää, I. Rajantie, S. Ylä-Herttuala, K. Alitalo, I.L. Weissman, and P. Salven. 2008. Bone marrow-derived circulating endothelial precursors do not contribute to vascular endothelium and are not needed for tumor growth. *Proc. Natl. Acad. Sci. USA.* 105:6620–6625. https://doi.org/10.1073/pnas.0710516105

Rafii, S., J.M. Butler, and B.S. Ding. 2016. Angiocrine functions of organ-specific endothelial cells. *Nature.* 529:316–325. https://doi.org/10.1038/nature17040

Scholten, D., J. Trebicka, C. Liedtke, and R. Weiskirchen. 2015. The carbon tetrachloride model in mice. *Lab. Anim.* 49(1, Suppl):4–11. https://doi.org/10.1177/0023677215571192

Shi, Q., S. Rafii, M.H. Wu, E.S. Wijelath, C. Yu, A. Ishida, Y. Fujita, S. Kothari, R. Mohle, L.R. Sauvage, et al. 1998. Evidence for circulating bone marrow-derived endothelial cells. *Blood.* 92:362–367.

Spahr, L., Y. Chalandon, S. Terraz, V. Kindler, L. Rubbia-Brandt, J.L. Frossard, R. Breguet, N. Lanthier, A. Farina, J. Passweg, et al. 2013. Autologous bone marrow mononuclear cell transplantation in patients with decompensated alcoholic liver disease: a randomized controlled trial. *PLoS One.* 8:e53719. https://doi.org/10.1371/journal.pone.0053719

Verbiest, T., R. Finnon, N. Brown, P. Finnon, S. Bouffler, and C. Badie. 2016. NOD scid gamma mice are permissive to allogeneic HSC transplantation without prior conditioning. *Int. J. Mol. Sci.* 17:E1850. https://doi.org/10.3390/ijms17111850

Wakabayashi, T., H. Naito, J.I. Suehiro, Y. Lin, H. Kawaji, T. Iba, T. Kouno, S. Ishikawa-Kato, M. Furuno, K. Takara, et al. 2018. CD157 marks tissue-resident endothelial stem cells with homeostatic and regenerative properties. *Cell Stem Cell.* 22:384–397.e6. https://doi.org/10.1016/j.stem.2018.01.010

Wang, L., X. Wang, G. Xie, L. Wang, C.K. Hill, and L.D. DeLeve. 2012. Liver sinusoidal endothelial cell progenitor cells promote liver regeneration in rats. *J. Clin. Invest.* 122:1567–1573. https://doi.org/10.1172/JCI58789

Waskow, C., V. Madan, S. Bartels, C. Costa, R. Blasig, and H.R. Rodewald. 2009. Hematopoietic stem cell transplantation without irradiation. *Nat. Methods.* 6:267–269. https://doi.org/10.1038/nmeth.1309

Zhang, M., A.B. Malik, and J. Rehman. 2014. Endothelial progenitor cells and vascular repair. *Curr. Opin. Hematol.* 21:224–228. https://doi.org/10.1097/MOH.0000000000000041